

# Black Hole Mass Estimates of Radio Selected Quasars

A. Y. K. N. Oshlack,

*School of Physics, University of Melbourne, Parkville, Victoria 3010, Australia*

`aoshlack@physics.unimelb.edu.au`

R. L. Webster

*School of Physics, University of Melbourne, Victoria 3010, Australia*

`rwebster@physics.unimelb.edu.au`

and M. T. Whiting

*School of Physics, University of Melbourne, Victoria 3010, Australia*

`mwhiting@physics.unimelb.edu.au`

## ABSTRACT

The black hole (BH) mass in the centre of AGN has been estimated for a sample of radio-selected flat-spectrum quasars to investigate the relationship between BH mass and radio properties of quasars. We have used the virial assumption with measurements of the  $H\beta$  FWHM and luminosity to estimate the central BH mass. In contrast to previous studies we find no correlation between BH mass and radio power in these AGN. We find a range in BH mass similar to that seen in radio-quiet quasars from previous studies. We believe the reason that the low BH mass radio-loud quasars have not been measured in previous studies is due to optical selection effects which tend to miss the less optically luminous radio-loud sources.

*Subject headings:* galaxies: active—galaxies: nuclei—quasars: general

## 1. Introduction

Although it is commonly accepted that quasars harbor a super-massive black hole (BH) in their core, neither the distribution of the physical characteristics of these BHs, nor their

relationship to other properties of quasars is clear. In this paper we further explore the connection between BH mass and radio luminosity in a quasar.

Recently a range of methods have been used to determine the BH masses in galaxies and quasars. For nearby galaxies, stellar velocity dispersions and high resolution optical images are used to determine the BH and bulge masses. Recently a tight correlation between BH mass and velocity dispersion in the bulge of galaxies has been found ( $M_{BH} - \sigma$  relation: Gebhardt et al. 2000; Ferrarese & Merritt 2000). In addition there is evidence that the mass of the bulge component of the host galaxy correlates with BH mass (Kormendy & Richstone 1995; Magorrian et al. 1998). In AGN, it is difficult to determine BH mass using host galaxy dynamics or structure as the nucleus swamps the light from the host galaxy. Also since the redshifts are large, the projected sizes of the host galaxies are relatively small. Therefore indirect methods have been developed to measure BH mass in quasars.

The mass of the BH in a quasar can be estimated using the virial technique. Laor (1998) assumed that the  $H\beta$ -emitting clouds in the broad line region (BLR) are virialized, and then required only estimates of the radius of the  $H\beta$ -emitting region and the rotational velocity of that region to determine the mass. In quasars, the radius of the BLR has also been estimated using reverberation techniques. This method tracks intensity variations in the continuum luminosity which, a certain time later, are reflected in the emission line flux. This time lag is interpreted as the light travel time between the core of the quasar and the broad emission line region and therefore gives the radius of the broad line clouds from the central continuum source. Reverberation mapping measurements have been restricted to a few dozen Seyferts and quasars as they require intensive regular monitoring over periods of years and highly variable quasars. The quasars so far studied may not represent the broader AGN population. Regardless of this, these observations give extremely interesting results. The time delay for different ionization species provides strong support for photoionization of the broad line region and evidence that the kinematics of the broad line region is dominated by the central BH (Peterson & Wandel 2000).

The BLR clouds are assumed to have velocities related to the widths of the broad emission lines so if the velocities of the clouds are assumed to be Keplerian, the mass of the central BH can be deduced. Several low luminosity quasars have been studied using both reverberation techniques and galactic velocity dispersion to measure their BH mass (Ferrarese et al. 2001). These results show that both these methods give consistent BH masses and that the  $M-\sigma$  relation holds for both active and non-active galaxies.

Estimates of the BH masses of radio-loud quasars have been published for several samples. (Laor 2000) used the Palomar-Green sample of quasars (PG; Remillard et al. 1991) with spectra provided by Boroson & Green (1992) to deduce that a relatively powerful jet

requires a BH with mass  $M_{BH} > 3 \times 10^8 M_{\odot}$ . The key point Laor makes is that the BH mass does not depend on radio luminosity, but on the radio luminosity *relative* to the optical luminosity (denoted by the ratio  $\mathcal{R}$ ). The PG sample comprises quasars selected for their UV-excess, and a limiting magnitude  $B \lesssim 16.6$  giving a population biased towards low redshift quasars.

Gu, Cao, & Jiang (2001) consider a sample of very radio-loud quasars taken from the 1Jy, S4 and S5 catalogues. They estimate the BH masses for these quasars also using the virial technique. They are able to divide their sample into steep spectrum and flat spectrum sources and find that the distribution of properties is similar for both subsets. They find 7 out of their 86 sources have BH masses  $< 10^8 M_{\odot}$  unlike previous authors (eg, Laor 2000). In another carefully matched sample of radio-galaxies, radio-loud and radio-quiet quasars, Dunlop et al. (2001) show that the host galaxies of each class of AGN are nearly indistinguishable. However these authors confirm the Laor (2000) result that radio-loud quasars have BH masses  $\gtrsim 10^9 M_{\odot}$ .

A second line of enquiry relates radio continuum emission to the mass of the BH. Lacy et al. (2001) used the First Bright Quasar Survey (FBQS; White et al. 2000) in their analysis. These quasars are the optically brightest ( $R \leq 17.8$ ), blue ( $B - R \leq 2.0$ ) quasars in a radio sample selected at  $\lambda = 20cm$ . These authors obtained a best fit relation

$$\log L_{5GHz} = 1.9 \text{Log} M_{BH} + 1.0 \log \left( \frac{L}{L_{Edd}} \right) + 7.9 \quad (1)$$

giving a continuous, monotonic, dependence of radio luminosity on BH mass. These studies used the virial estimator for BH mass. This is similar to the result by Franceschini, Vercellone & Fabian (1998) who found a very steep dependence of BH mass on radio flux,  $P_{5GHz} \propto M_{BH}^{2.5}$ , and attributed this to BH accretion in an advection dominated accretion flow.

Most recently Ho (2002) has compiled a complete list of BH measurements which use robust methods to determine mass (stellar dynamics, reverberation mapping or maser dynamics). He finds that the BH mass shows little dependence on  $\mathcal{R}$  and that the radio luminosity correlates poorly with BH mass.

We have been studying the properties of the Parkes Half-Jansky flat-spectrum Sample (PHFS; Drinkwater et al. 1997), to better understand the emission mechanisms particularly at optical wavelengths. We find that the optical emission in radio quasars is a mixture of several different components: a blue component similar to the ‘big blue bump’ in optically-selected quasars, which is presumed to photoionize the BLR, plus a synchrotron component which turns over somewhere in the optical-to-IR and is a significant contributor to the optical emission in a large fraction of sources (Whiting, Webster, & Francis 2001). Two major differences between our sample and those already published are (1) our sample is

completely identified in the optical, and we have not selected optically bright sources, and (2) our sources are flat spectrum, which suggests that the radio flux may be boosted by orientation effects.

In section 2, we discuss the method used for estimation of BH mass from measured optical parameters. In section 3, we describe our application of these techniques to the PHFS dataset. Results and discussion are given in section 4. Where required, a cosmology with  $H_0 = 75 \text{ km s}^{-1} \text{ Mpc}^{-1}$  and  $q_0 = 0.5$  is assumed.

## 2. Method

When the motions of the gas moving around the BH are dominated by the gravitational forces, virial estimates of the BH mass can be made based on the radius and velocity of this gas using  $M_{BH} = rv^2G^{-1}$ . There is evidence that the BLR gas emitting the  $H\beta$  line is virialized (Peterson & Wandel 2000). To estimate BH masses for this sample, we follow the work of Kaspi et al. (2000) who used reverberation mapping to derive an empirical relationship between radius and luminosity. To determine  $v$ , the rotational velocity, we correct full-width half-maximum  $v_{FWHM}$  of the  $H\beta$  emission line by a factor of  $\sqrt{3}/2$  to account for random orientation affecting the width of emission lines. The assumption of random orientation is discussed further in Section 4.2. The mass is then

$$M = 1.464 \times 10^5 \left( \frac{R_{BLR}}{\text{lt-days}} \right) \left( \frac{v_{FWHM}}{10^3 \text{ km s}^{-1}} \right)^2 M_{\odot} \quad (2)$$

The empirical relation of Kaspi et al. (2000) relates the radius of the emission lines to the continuum luminosity of the source:

$$R_{BLR} = (32.9) \left[ \frac{\lambda L_{\lambda}(5100\text{\AA})}{10^{44} \text{ erg s}^{-1}} \right]^{0.700} \text{ lt-days} \quad (3)$$

with an error in the fitted slope of this relation of  $< 5\%$ . This correlation holds above a luminosity of  $10^{44} \text{ erg s}^{-1}$ . Below this value the correlation is less certain and at low luminosity most values of the emission line region radius lie well below the linear relation, which would lead to an even lower estimate of the BH mass.

Although the slope of this relation cannot be explained theoretically, the radius of the BLR is approximately linear with the strength of the radiation field ionizing the BLR gas. Therefore, to use the  $H\beta$  BH mass estimator, two measurements are involved. Firstly, the luminosity at  $5100\text{\AA}$  and secondly, the  $H\beta$  FWHM.

### 3. PHFS Data

The data used in the analysis are taken from the PHFS (Drinkwater et al. 1997). The selection criteria for the sample are: (1) Radio loud: 2.7GHz flux  $> 0.5$  Jy; (2) Flat spectrum taken from the 2.7 GHz and 5 GHz fluxes:  $\alpha > -0.5$ , where  $S_\nu \propto \nu^\alpha$ ; (3) Dec range +10 to  $-45$  and galactic latitude  $|b| > 10^\circ$ . The selection criteria produced 323 radio sources where optical identification has been made for 321 sources. Therefore the sample has no optical selection criteria. The flat spectrum criterion may mean that sources where the radio jets are predominantly oriented towards us are preferentially selected. Most of the radio morphologies are compact.

For the PHFS, estimating the optical luminosity of the quasar is difficult as there is a very large range in colour for the sources (Francis, Whiting, & Webster 2000). This means we cannot use a general K-correction for all the objects. In the initial plots we will use the  $B_j$  magnitude to calculate the luminosity. The error in the  $B_j$  magnitudes from the COSMOS catalogue is quoted as being  $\pm 0.5$  magnitudes, but Drinkwater et al. (1997) have found that some fields seem to be in error by more than one magnitude. This produces an error in the BH mass estimates of about a factor of 2. Given that the range of masses covers 4 orders of magnitude, these errors are not critical. In section 4.2 we only consider the subset of quasars which have more accurate magnitudes. The radio flux of the sources given in Drinkwater et al. (1997) comes from the Parkes catalogue (PKSCAT90, Wright & Otrupcek (1990)) at 5GHz. It should also be noted that there is a large range in  $B_j$  magnitudes, including very faint sources which have luminosities in the Seyfert regime.

187 sources in the sample have low to moderate resolution spectra (discussed in Francis et al. (2001)). Of these 101 were obtained at the AAT and Siding Spring 2.3m telescopes (Drinkwater et al. 1997), and 86 are from the compilation of Wilkes et al. (1983). The quality and wavelength coverage of the spectra is diverse; many have low resolution and signal-to-noise. Estimates of the likely errors are further discussed in the next section.

All spectra with a wavelength range covering  $H\beta$  were used in the analysis. This gave a list of 39 quasars. Each  $H\beta$  emission line was fitted by a Gaussian and Lorentzian using the *splot* package in IRAF. If  $H\beta$  was outside the observed wavelength range but  $H\alpha$  was observed then the fit was done for  $H\alpha$ . The Lorentzian fits were better approximations to the line shapes by eye. The Gaussian fits consistently underestimated the peak flux; therefore Lorentzian fits had consistently lower FWHMs. In the analysis we used the Lorentzian fits for measurements of the line widths. The errors in the estimation of  $v_{FWHM}$  are of the order of 10-20%. Where there was both the  $H\beta$  and  $H\alpha$  lines measured we calculated the BH mass using both values for the FWHM. The results of this is shown in Figure 1. It can be seen that the  $H\alpha$  widths give consistently lower BH masses, on average, 0.157 dex lower.

Therefore a correction of  $10^{0.157}$  was made to all BH masses estimated using  $H\alpha$ .

The radio loudness parameter  $\mathcal{R}$  is defined by  $f_\nu(5GHz)/f_\nu(5100\text{\AA})$ . A value of  $\mathcal{R} = 10$  is usually taken as the break in a bimodal distribution, dividing radio-loud and radio-quiet. All the PHFS sources are clearly radio-loud with  $10^2 < \mathcal{R} < 10^5$ . Table 1 gives the observed parameters for each source.

## 4. Results and Discussion

Considerable care must be exercised in searching for correlations between observed and derived quantities, particularly when the plotted quantities both depend in a similar way on distance. As an example, in a radio flux-limited sample, most quasars have a flux near the sample limit. Therefore two quantities which depend on distance will be correlated, including BH mass calculated from the virial estimator described above, which uses the absolute luminosity.

### 4.1. Correlations with Black Hole Mass

Figure 2 plots  $\mathcal{R}$ , the ratio of radio to optical flux, against the BH mass of each quasar. Contrary to some previous results but consistent with Ho (2002), we find a large range in derived BH masses. The apparent anti-correlation here is a consequence of using the optical flux in the measurement of BH mass and also using it in the calculation of  $\mathcal{R}$ . A significant fraction of the masses are well below limit of  $3 \times 10^8 M_\odot$  suggested by Laor (2000) as a necessary condition for radio-loud quasars. In fact, the range in BH masses is similar to the radio-quiet population of the PG quasar sample (Laor 2000). For 8 of the AGN the host galaxies are visible but it is clear from figure 2, where these galaxies are marked with a ‘g’ or ‘G’, that these are not the only low BH mass. In these cases we expect the quasar luminosity to be over-estimated, due to the inclusion of galaxy flux. The likely increase in flux is  $< 50\%$  (Masci, Webster, & Francis 1998). Only two of the sources have redshifts  $< 0.1$ .

A histogram of the BH mass is shown in Figure 3. The low values for the BH mass are a direct consequence of the low optical luminosities, with the range in the width of the  $H\beta$  emission line introducing some scatter. This dependence is clearly shown in Figure 4 where the optical luminosity is plotted against the BH mass, and there is no evidence of a lower limit in either optical luminosity or BH mass for any of these radio-loud quasars.

Figure 5 shows the relationship between radio power and BH mass. There is no clear relationship between these variables unlike the results of Franceschini, Vercellone & Fabian

(1998) and Lacy et al. (2001). The fact that we are not seeing a relationship between BH mass and radio power is a consequence of the fact that there isn't a tight correlation between optical luminosity and radio luminosity in quasars (Stern et al. 2000; Wadadekar & Kembhavi 1999). This has been investigated by Hooper et al. (1996) for the LBQS who find that the distribution of radio luminosity does not depend on absolute magnitude over most of the range of  $M_B$ . Furthermore the PG survey used by Laor (2000) differs from this and other optically selected samples in its population of radio-loud quasars with respect to optical luminosity (Hooper et al. 1996). The PG sample contains a higher fraction of radio-loud quasars which have bright absolute magnitudes compared to other surveys like the LBQS (Hooper et al. 1996). If we consider Figure 2 in Ho (2002), then our data points lie in the underpopulated upper left region of this plot. This confirms Ho's conclusion that there is no obvious relationship between these two variables. However we note that our sources are flat spectrum and the radio-flux may be boosted by beaming which would tend to increase the value of  $\mathcal{R}$ . Also included in Figure 5 is a line of constant observed flux. This is included to demonstrate the correlation that would be observed for objects with the same measured flux (eg: the flux limit of the sample where the majority of object will be selected) at the different redshifts of the sources.

#### 4.2. Possible Biases in Estimates of Parameters

There are two measurements involved in deriving the BH mass for any object while using this method: firstly the optical flux, to derive the radius to the BLR and secondly the velocity width,  $v_{FWHM}$  used for the velocity component in the virial assumption. There are several factors which might affect the applicability of the virial method to the quasars we are considering.

1. All the sources in this sample are flat spectrum. One might speculate that the radio emission in particular is beamed, increasing the radio flux relative to the optical. The effect of the beaming would be that the points in Figure 2 are at higher  $\mathcal{R}$  values than their non-beamed values, but this should be independent of BH mass unless the latter also effects the Lorentz factor of the jet. Interestingly, in a recent preprint, Gu, Cao, & Jiang (2001) have shown using a similar sample to the PHFS, that steep and flat spectrum quasars have similar distributions of BH mass compared to radio luminosity and radio loudness  $\mathcal{R}$ .
2. The spectral energy distributions (SEDs) for radio-loud quasars vary greatly, making a uniform K-correction invalid. This means that for quasars at different redshifts we are sampling different parts of the spectrum by using the  $B_j$  magnitude.

To investigate this effect, we can use 24 of the quasars with measured velocity profiles which also have quasi-simultaneous photometry in seven bands covering the optical and near IR (Francis, Whiting, & Webster 2000). Four of these have evidence for dust reddening which is discussed further in item 4. The original BH mass distribution of these 20 unreddened quasars is shown in Figure 6a. Using the simultaneous photometry we can now linearly interpolate between these SED data points to obtain an accurate flux at a rest wavelength of  $5100\text{\AA}$ . The histogram of the results is shown in Figure 6b. The range in BH masses has decreased, and the lower limit proposed by Laor (2000) is even more strongly violated.

3. It has been shown that the synchrotron radiation from the jet can extend into the near IR and optical (Whiting, Webster, & Francis 2001). This will cause an increase in the observed continuum flux but, since the jet emission is beamed, would not contribute to the ionizing flux seen by the BLR. Whiting, Webster, & Francis (2001) have fitted models to the quasi-simultaneous photometry that consist of both a synchrotron component and a blue powerlaw (representing the ionizing flux from the accretion disk). From these fits we can calculate the fraction of the total emission that comes from the accretion disk. The accretion disk flux will be less than the observed flux if there is a significant synchrotron contribution present in the optical. The results of this correction are shown in Figure 6c where some of the objects with a large synchrotron component now have much lower BH masses. Nearly all the quasars are below  $10^9 M_{\odot}$ .
4. Dust may affect the observed luminosity of the quasar. Dust will tend to redden the spectrum of the quasar and reduce the observed luminosity. The dust extinction is modeled as an exponential function of wavelength with flux at the blue wavelengths depleted significantly more than the red. For quasars where we have simultaneous photometry, evidence of dust is shown by a steep decrease in flux at higher energies. For the subset of quasars that have photometry we see evidence of dust in the SEDs of four of the quasars. We have not used these quasars in the previous analysis as their flux will be underestimated. After removing these, we still see the very large range in BH masses including low mass BHs.
5. The  $H\beta$  line might be emitted from a disk-like structure, with its line width reflecting the rotation of that disk (Wills & Browne 1986). Then, since it is expected that flat spectrum sources are viewed face-on, the width of the  $H\beta$  line may be underestimated. In the Gu, Cao, & Jiang (2001) sample the median and mean values for their flat spectrum sample are lower than the steep spectrum sample. This data partially supports the flattened disk scenario (see Table 2). However it cannot be the whole story as the widths of the emission lines of the flat spectrum quasars are still a significant fraction



of the steep spectrum ones and, the flat-spectrum sources need only to be oriented at an average angle of  $53^\circ$  to the line-of-sight to reconcile to difference in the median values of FWHM. If we use the Gu, Cao, & Jiang (2001) difference, this introduces a mean difference of a factor of 2 in the BH mass.

6. Contamination of the AGN by the host galaxy light will effect all AGN to some extent, however it is obviously more significant for the objects where the host galaxy is resolved optically. The flux measured is the integrated flux over the entire galaxy. The central source flux which is required to calculate the BH mass, is much smaller. This effect will be present for all objects, but where the galaxy is resolved it will be the most pronounced as the host galaxy is a bigger percentage of the total observed flux. The result will be that the actual BH mass, for the AGN, is quite a bit smaller than calculated, so these masses are upper limits. The FWHM of the emission lines may also be effected by the host galaxy if it has strong  $H\alpha$  or  $H\beta$  emission lines. As we haven't resolved the broad and narrow components of the emission, the FWHM may be under-estimated due to a higher peak coming from the host galaxy emission. This is more likely to be a factor in the  $H\alpha$  emission lines. The resolution of the spectra was not sufficient to consider contamination by weaker nearby emission lines such as Fe II and N II. It is noted that the FWHM velocity of the  $H\beta$  line, after deconvolution, would need to increase by a factor of 10 to be consistent with the Laor (2000) finding - an unlikely result.

### 4.3. Optical Properties of Quasars

The results suggest that BH mass is not connected to the radio-loudness of the objects. The question then arises: Why have studies in the past produced a different result? Figure 4 shows that the range in values that we calculate for the BH mass is largely a consequence of using the optical luminosity to estimate the radius of the BLR. The velocity width of the lines has a much smaller effect on the BH mass distribution due to its smaller dynamic range. Therefore, the reason that previous studies using this method have missed the low BH mass radio-loud objects is because they have missed the low luminosity radio-loud objects. We believe that optical selection is biased against selecting low optical luminosity, radio-loud quasars as shown in the PG sample (Hooper et al. 1996).

The selection criterion for the low redshift PG quasars used by Laor (2000) are: (1) UV excess ( $U-B < -0.44$ ). (2) morphological criteria where the objects must have a 'dominant star-like appearance'. They are also bright with a limiting magnitude  $\sim 16.6$ . Therefore we obtain a sample of bright, blue, point-like objects. The key difference in the PHFS and the

sample used by Laor (2000) is that the PHFS has a large range in optical luminosity which produces the large distribution in BH mass whereas the radio-loud quasars selected on UV excess tend to have the characteristic of being optically luminous which therefore gives large BH masses. From the PHFS it is evident that not all radio-loud quasars are highly optically luminous.

Figure 7 provides evidence of an additional correlation which might effect selection into quasar samples. In figure 7, which plots optical luminosity against colour (B-I), low luminosity quasars are shown to be redder. Thus any additional selection criterion based on colour will further bias against low luminosity quasars. The photometry of these red quasars indicates that there are three types of reddening taking place. We find that a proportion of these are red due to synchrotron extending into the optical part of the spectrum and therefore boosting the red end of the continuum. This has been discussed and corrected for in section 4.2. This is an effect that will only be evident in radio-loud quasars with high energy synchrotron jets and will not be observed in radio-quiet quasars. Another subset of the redder objects in the PHFS have a substantial fraction of galactic light included in the photometry so the 4000Å break contributes to the red colour. This occurs mainly in the low redshift population which is a small subsample of our estimated BH masses. Most of the sources classified as ‘g’ or ‘G’ in Figure 2 do not have a significant galactic contribution in their spectra (for example, a significant 4000Å break), and are obviously AGN due to their strong radio loudness and broad emission lines. A smaller proportion of the sample are very faint and show some evidence of dust reddening where the blue end of the continuum is strongly suppressed. In this case the BH masses will be underestimated but the previous two effects lead to overestimation of the BH mass. Using the simultaneous photometry we have identified 4 out of 24 dust-reddened objects in the sample and have excluded them in the analysis shown in Figure 6: we still get a population of quasars with relatively low BH mass.

Why do red quasars have low optical luminosity, and therefore (under our assumptions), low BH mass? We have argued that a significant fraction of red quasars have synchrotron turning over at optical wavelengths (Whiting, Webster, & Francis 2001). This seems to be correlated with lower optical emission which could be interpreted in two ways. Either, the synchrotron emission remains unchanged but appears dominant only when the blue disk emission is low, or secondly, when the blue disk emission is low, relatively more energy goes into the jet and the synchrotron is increased. We do not have a large enough sample to establish the correlation between low luminosity and redness unequivocally, but if the correlation could be substantiated it might provide physically interesting constraints on the jet formation mechanism.

Theoretical calculations considered by Meier (1999) demonstrate explicitly that it is not necessary to have a relatively massive BH to produce powerful radio jets. In his model, based on current accretion and jet-production theory, the strength of the radio emission is tied to the rotation rate of the central BH. Therefore, it is quite possible to have highly powered radio jets with small BH masses if the BH is spinning rapidly.

## 5. Conclusion

The virial method for estimating BH mass in conjunction with the empirical relation between luminosity and radius (Kaspi et al. 2000) has been applied to the PHFS sample of flat spectrum radio sources. This is the first time the analysis has been applied to an optically complete radio-selected sample. The analysis is complimentary to the Ho (2002) analysis which concentrates on optically luminous sources used in longterm monitoring programs. The errors and applicability of this method have been discussed. The main result are summarized as follows:

1. We find no evidence for a lower cut off in the masses of radio-loud quasars as previously suggested in the literature.
2. The previous lower boundary on mass of radio-loud quasars was an optical selection effect. Low luminosity radio-loud AGN have been shown to have redder optical colours. These red quasars will be selected against in optical surveys.
3. We do not find any evidence for a relationship between radio properties and the BH mass of quasars. Further investigation of this relationship is hampered by unknown orientation effects.

To obtain more accurate BH estimates and improve our understanding of the relationship between the mass of the central BH and other properties of quasars, we need large samples of BH masses measured using the reverberation technique. This is now observationally possible using multi-fibre spectrographs.

We wish to acknowledge the anonymous referee for careful reading of the manuscript and valuable comments which lead to the improvement of this paper.

## REFERENCES

Boroson, T.A. & Green, R.F. 1992, *ApJS*, 80, 109

- Dietrich, M. et al. 1993, ApJ, 408, 416
- Drinkwater, M. J., Webster, R. L., Francis, P. J., Condon, J. J., Ellison, S. L., Jauncey, D. L., Lovell, J., Peterson, B. A., & Savage, A. 1997, MNRAS, 284, 85
- Dunlop, J. S., McLure, R. J., Kukula, M. J., Baum, S. A., O’Dea, C. P. & Hughes, D. H., submitted to MNRAS, astro-ph/0108397
- Ferrarese, L. & Merritt, D. 2000, ApJ, 539, L9
- Ferrarese, L., Pogge R. W., Peterson B. M., Merrit D., Wandel A. & Joseph C. L. 2001, ApJ, 555, L79
- Franceschini, A., Vercellone, S., & Fabian, A.C. 1998, MNRAS, 297, 817
- Francis, P. J., Whiting, M. T., & Webster, R. L. 2000, Publications of the Astronomical Society of Australia, 17, 56
- Francis, P. J., Drake, C. L., Whiting, M. T., Drinkwater, M. J., & Webster, R. L. 2001, Publications of the Astronomical Society of Australia, 18, 221
- Gebhardt, K. et al. 2000, ApJ, 539, L13
- Gelderman, R., & Whittle, M., 1994, ApJS, 91, 491
- Gu, M., Cao, X., & Jiang, D. R. 2001, MNRAS, 327, 1111
- Ho, L. C. 2002, ApJ, 564, 120.
- Hooper, E. J., Impey, C. D., Foltz, C. B., & Hewett, P. C. 1996, ApJ, 473, 746
- Kaspi, S., Smith, P. S., Netzer, H., Maoz, D., Jannuzi, B. T., & Giveon, U. 2000, ApJ, 533, 631
- Kellerman, K. I., Sramek, R., Schmidr, M., Shaffer, D. B., Green, R., 1989, AJ, 98, 1195
- Kormendy, J. & Richstone, D. 1995, ARA&A, 33, 581
- Lacy, M., Laurent-Muehleisen, S. A., Ridgway, S. E., Becker, R. H., & White, R. L. 2001, ApJ, 551, L17
- Laor, A. 1998, ApJ, 505, L83
- Laor, A. 2000, ApJ, 543, L111

- Magorrian, J. et al. 1998, AJ, 115, 2285
- Masci, F. J., Webster, R. L., & Francis, P. J. 1998, MNRAS, 301, 975
- Meier, D. L. 1999, ApJ, 522, 753.
- Peterson, B. M. & Wandel, A. 2000, ApJ, 540, L13
- Remillard, R. A., Grossan, B., Bradt, H. V., Ohashi, T. & Hayashida, K., 1991 Nature, 350, 589
- Schmit, M., & Green, R.F., 1983 ApJ, 269,352
- Stern, D., Djorgovski, S. G., Perley, R. A., de Carvalho, R. R., & Wall, J. V. 2000, AJ, 119, 1526
- Wadadekar, Y. & Kembhavi, A. 1999, AJ, 118, 1435
- White, R. L. et al. 2000, ApJS, 126, 133
- Whiting, M. T., Webster, R. L., & Francis, P. J. 2001, MNRAS, 323, 718
- Wilkes, B. J., Wright, A. E., Jauncey, D. L., & Peterson, B. A. 1983, Proceedings of the Astronomical Society of Australia, 5, 2
- Wills, B. J. & Browne, I. W. A. 1986, ApJ, 302, 56
- Wright, A. & Otrupcek, R. 1990, Parkes Catalog. Astralia Telescope National Facility, Epping (PKSCAT90) (113)

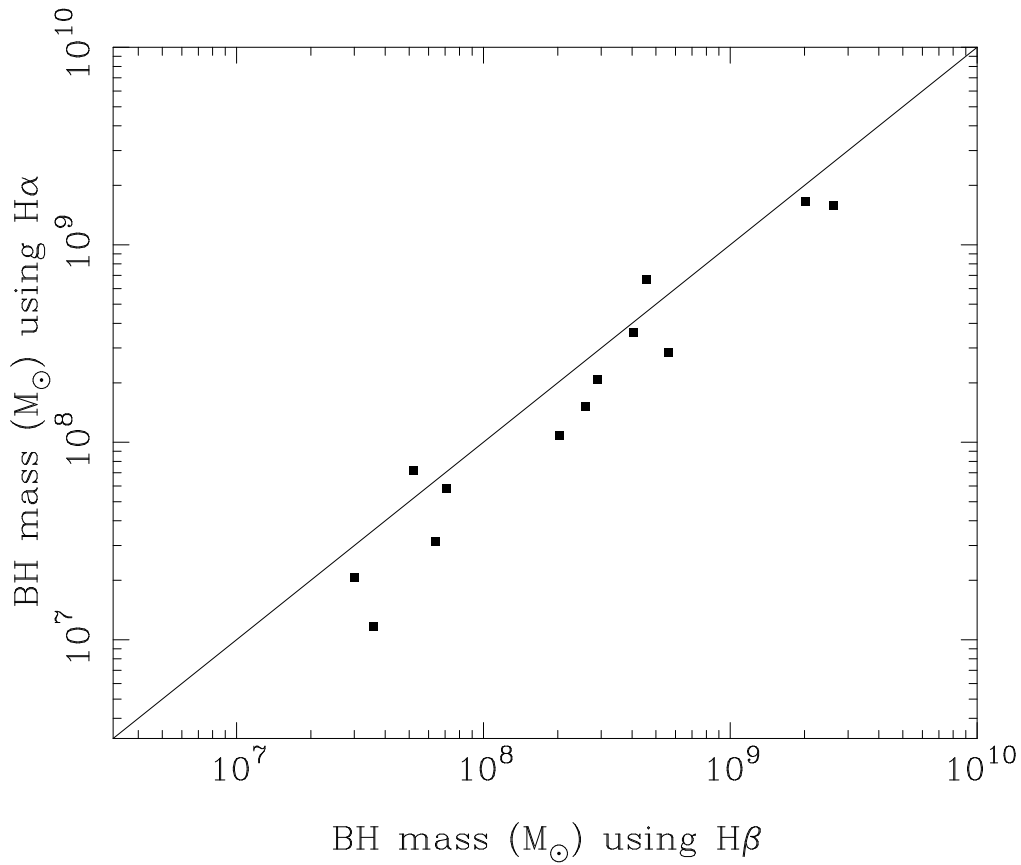


Fig. 1.— A comparison of BH masses estimated from using H $\alpha$  and H $\beta$  velocity widths for the same quasars. It can be seen that the BH estimates using H $\alpha$  are consistently lower by an average of 0.157 dex. The line represents equal BH mass.

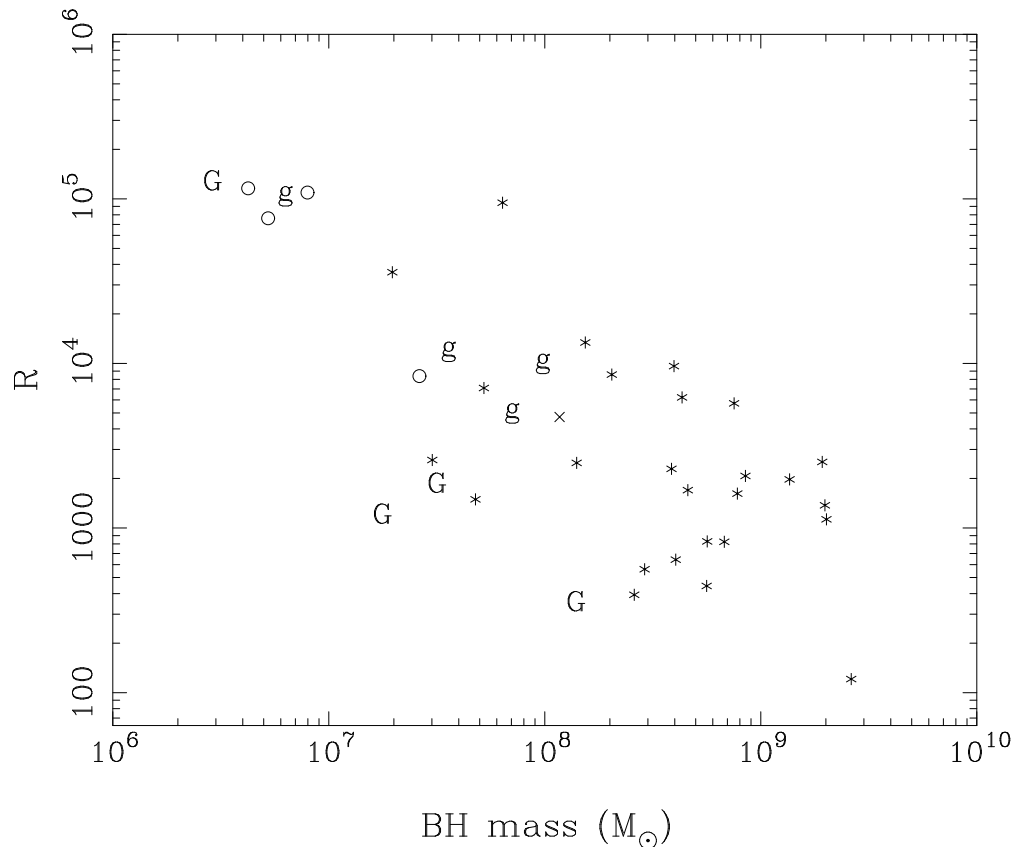


Fig. 2.— The BH mass vs  $\mathcal{R}$  (the ratio of radio to optical flux). This plot shows a large range in BH mass. The stars represent BH mass calculated using  $H\beta$  FWHM while the circles are calculated using  $H\alpha$  and the cross uses  $H\gamma$ . 8 of the objects in the sample have been classified as galaxies or merger events on the optical plates meaning that the host galaxy is visible. These objects have been represented with a ‘g’ when using  $H\beta$  to calculate the BH mass and a ‘G’ when using  $H\alpha$ . These objects also span a range at the lower end of BH mass.

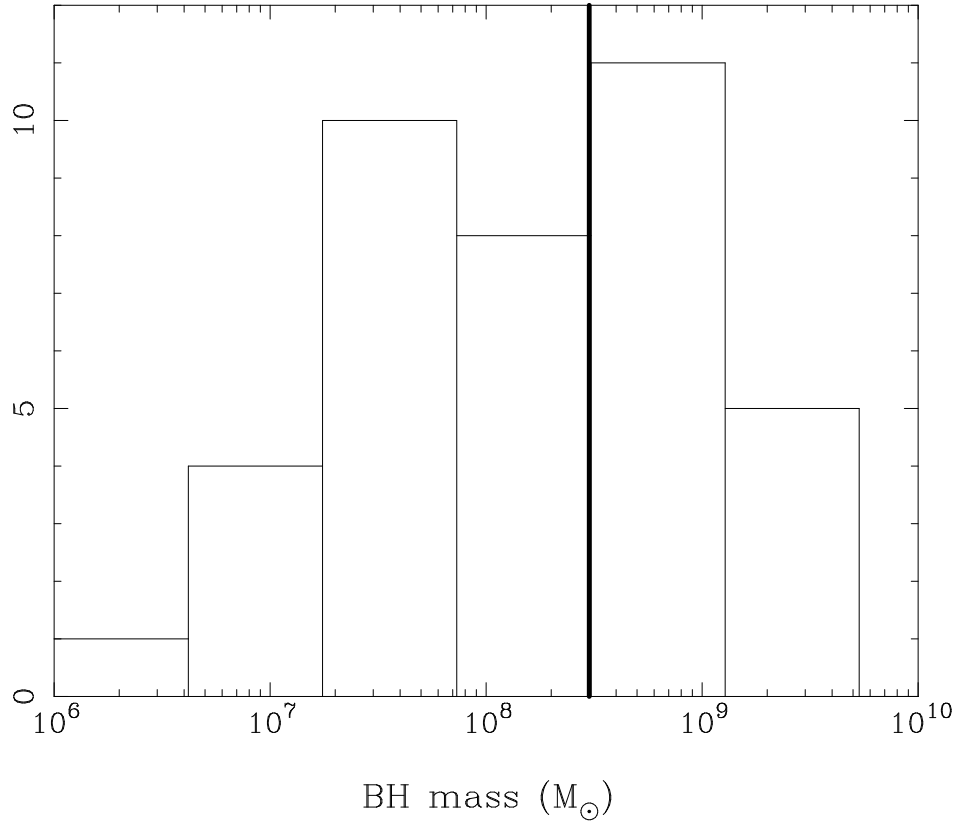


Fig. 3.— A histogram of the estimated BH mass for radio loud quasars from the PHFS. The solid line represents the lower limit to BH mass stated by Laor (2000) as necessary for having radio-loud quasars.



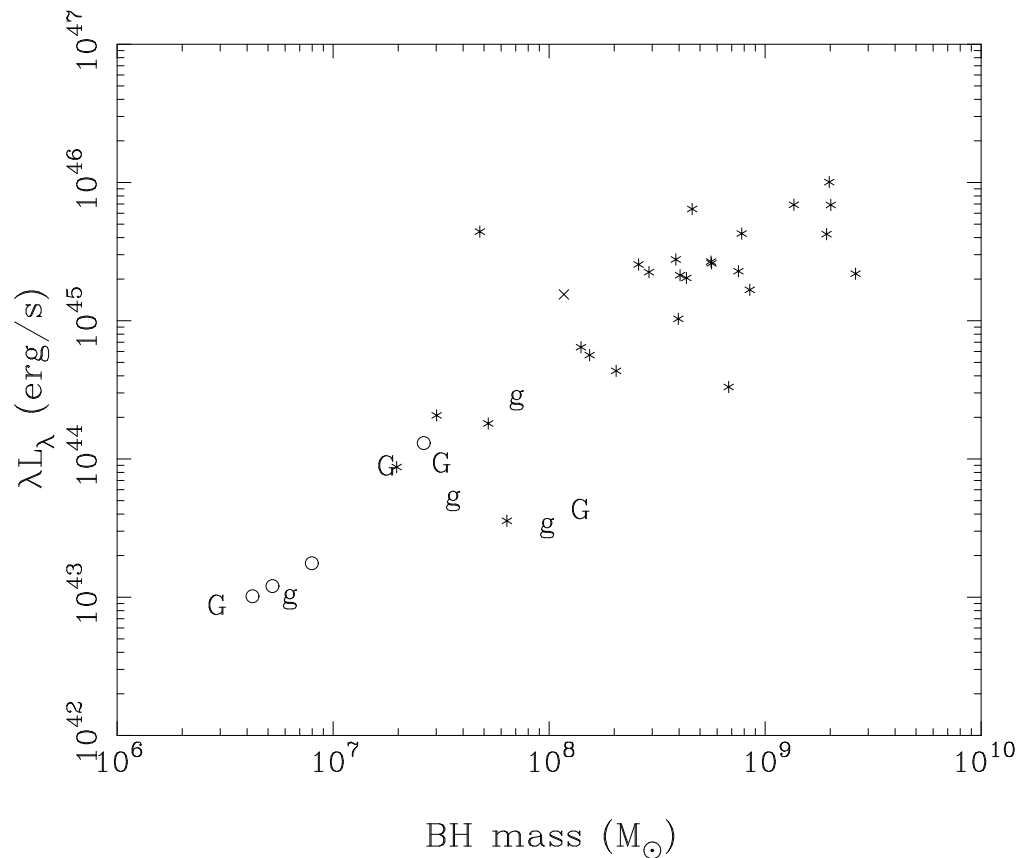


Fig. 4.— The correlation between BH mass and optical luminosity demonstrates the dependence of the virial estimate on the luminosity. It shows that the low BH mass quasars are a consequence of using the optical luminosity to estimate the radius of the emission line gas and the velocity width of the emission line only leads to a small scatter in the relation even though it has a higher order dependence in the virial assumption. The symbols as for Fig 2.

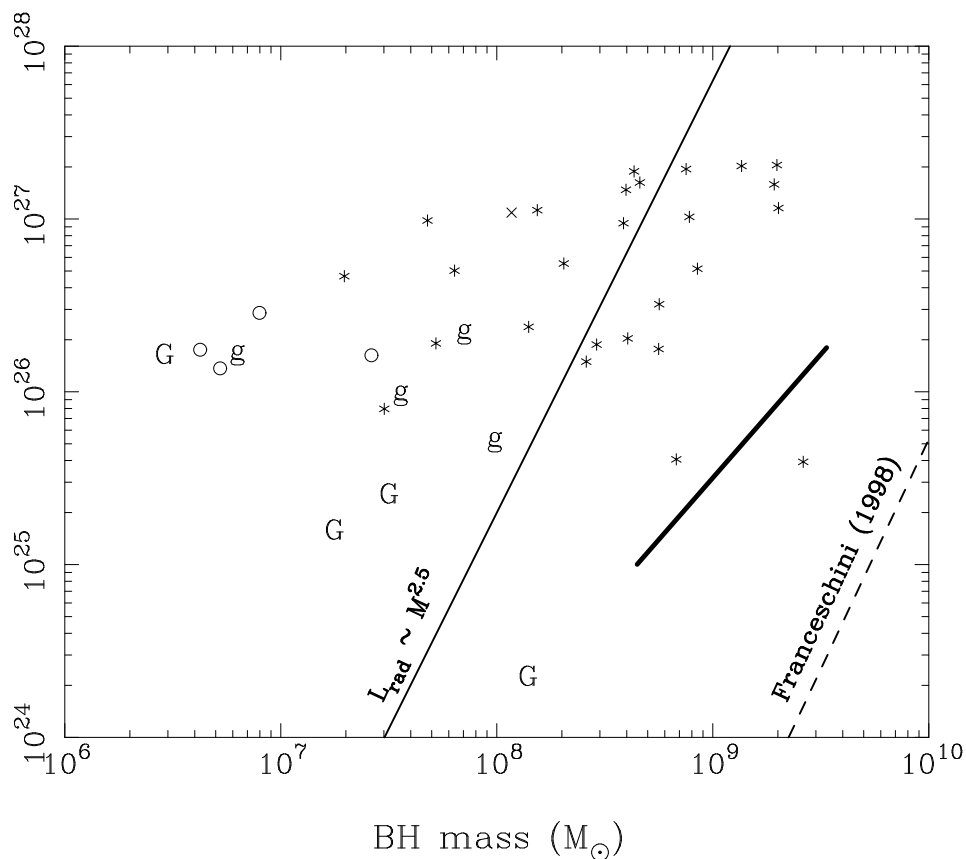


Fig. 5.— A plot of BH mass vs Radio power at 5 GHz. There is no evidence for a correlation or lower limit to the distribution. All the sources are powerful radio sources. The thick solid line represents constant, observed flux over different redshifts. The dashed line represents the correlation found by Franceschini, Vercellone & Fabian (1998) and the thin solid line corresponds to the radio power going like the BH mass to the power of 2.5 ( $L_{rad} \sim M_{\odot}^{2.5}$ ) similar to the upper boundary suggested by Dunlop et al. (2001). Symbols as for Figure 2.

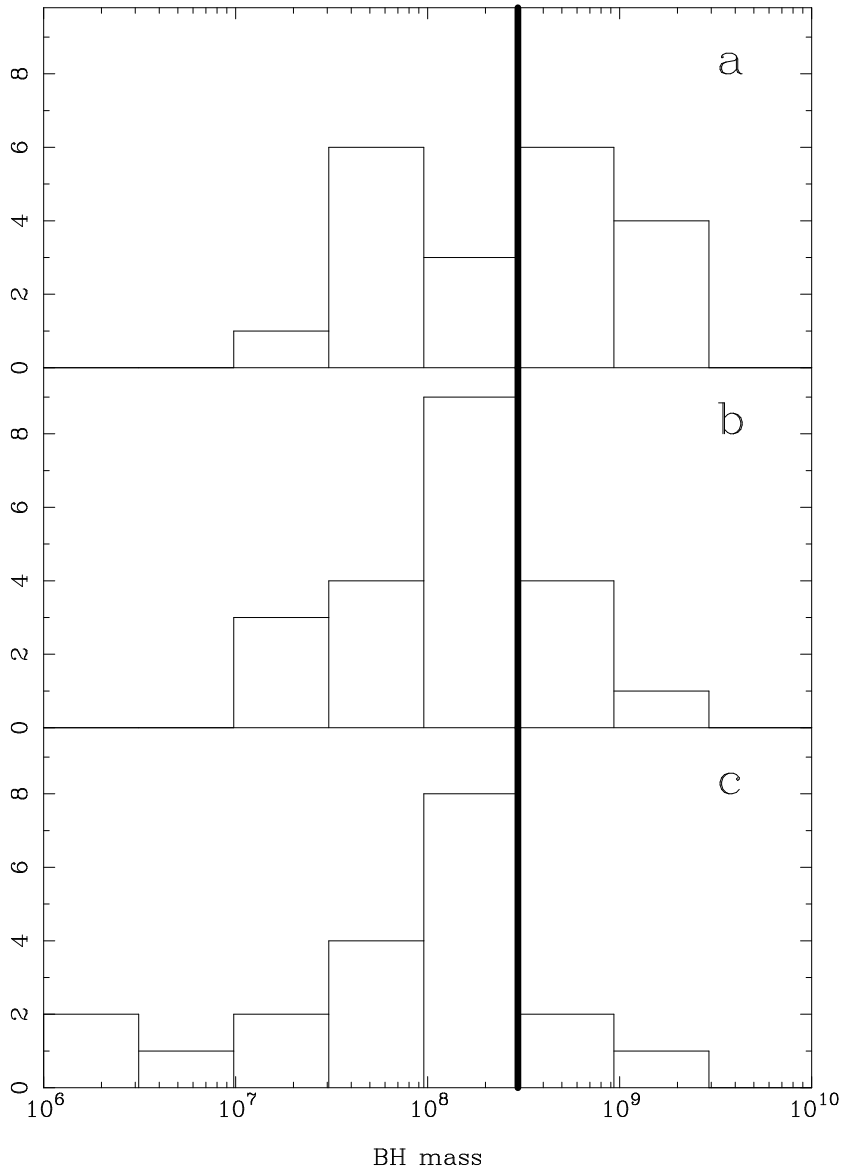


Fig. 6.— The histogram for BH masses of the 20 quasars that have quasi-simultaneous optical and near IR photometry. The four quasars that have SEDs that indicate dust reddening have been excluded. The photometry enables us to do a proper K-correction for the flux at  $5100\text{\AA}$ . The solid line represents the lower limit on the mass of BHs in radio-loud quasars suggested by Laor (2000). (a) shows the 20 quasars using the  $B_j$  magnitude to calculate the flux at  $5100\text{\AA}$ . (b) uses the simultaneous photometry to calculate the K-corrected flux at  $5100\text{\AA}$ . (c) uses fluxes corrected to take into account the fraction of the synchrotron that extends into the optical continuum calculated by Whiting, Webster, & Francis (2001).

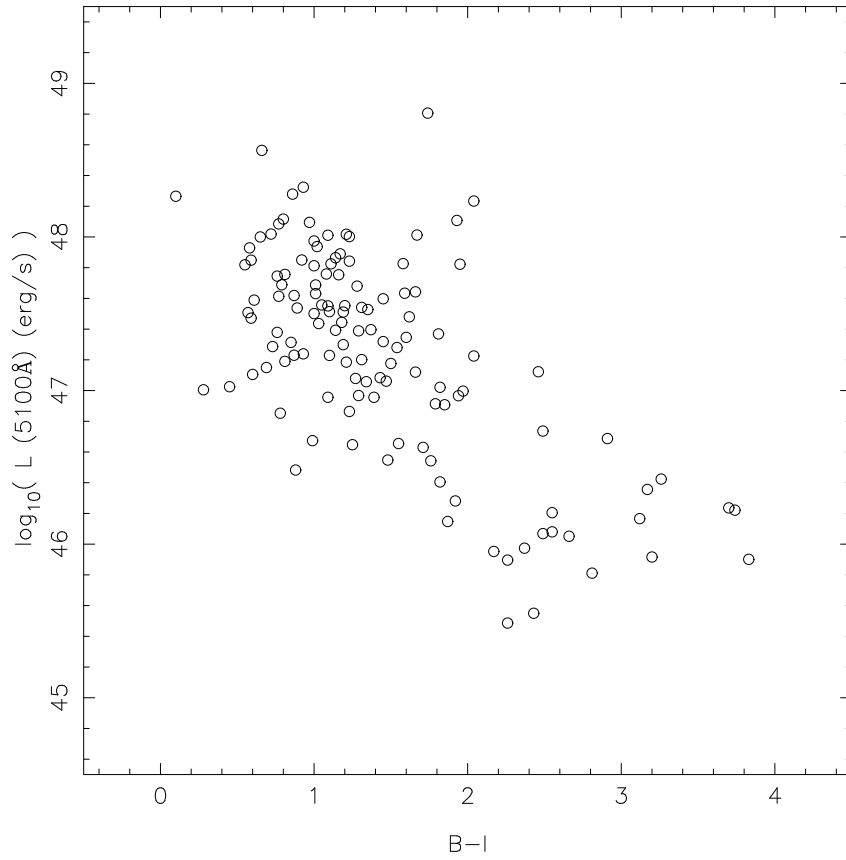


Fig. 7.— Colour vs Optical Luminosity plot for the whole PHFS with quasi-simultaneous photometry (Francis, Whiting, & Webster 2000). It shows that the redder objects are the ones with lower optical luminosity and would probably be missed in samples that have been selected based on optical colours or UV excess.

Table 1: Observational Data for PHFS Quasars and Estimated BH Mass

| Name         | $z$   | $B_j$ | $\lambda L_\lambda$<br>(ergs s <sup>-1</sup> ) | 5GHz<br>flux<br>(Jy) | $P_{rad}$<br>(5GHz)<br>(W/Hz) | $\mathcal{R}$      | H $\beta$<br>FWHM<br>( $km s^{-1}$ ) | H $\alpha$<br>FWHM<br>( $km s^{-1}$ ) | BH mass<br>( $M_\odot$ ) |
|--------------|-------|-------|--|----------------------|-------------------------------|--------------------|--------------------------------------|---------------------------------------|--------------------------|
| PKS 0114+074 | 0.343 | 22.14 | $1.05 \times 10^{43}$                          | 0.67                 | $1.74 \times 10^{26}$         | $1.11 \times 10^5$ | 2515                                 | ...                                   | $6.30 \times 10^6$       |
| PKS 0153-410 | 0.226 | 19.41 | $5.41 \times 10^{43}$                          | 0.94                 | $1.02 \times 10^{26}$         | $1.26 \times 10^4$ | 3385                                 | 1932                                  | $3.59 \times 10^7$       |
| PKS 0221+067 | 0.510 | 20.76 | $8.75 \times 10^{43}$                          | 0.77                 | $4.66 \times 10^{26}$         | $3.59 \times 10^4$ | 2118                                 | ...                                   | $1.97 \times 10^7$       |
| PKS 0327-241 | 0.888 | 19.39 | $1.03 \times 10^{45}$                          | 0.73                 | $1.48 \times 10^{27}$         | $9.63 \times 10^3$ | 4007                                 | ...                                   | $3.96 \times 10^8$       |
| PKS 0454+066 | 0.405 | 19.79 | $1.30 \times 10^{44}$                          | 0.44                 | $1.63 \times 10^{26}$         | $8.39 \times 10^3$ | ...                                  | 2128                                  | $3.77 \times 10^7$       |
| PKS 0502+049 | 0.954 | 18.7  | $2.28 \times 10^{45}$                          | 0.82                 | $1.94 \times 10^{27}$         | $5.73 \times 10^3$ | 4184                                 | ...                                   | $7.53 \times 10^8$       |
| PKS 0912+029 | 0.427 | 19.56 | $1.80 \times 10^{44}$                          | 0.46                 | $1.90 \times 10^{26}$         | $7.10 \times 10^3$ | 2678                                 | 3152                                  | $5.23 \times 10^7$       |
| PKS 0921-213 | 0.052 | 16.4  | $4.25 \times 10^{43}$                          | 0.42                 | $2.23 \times 10^{24}$         | $3.53 \times 10^2$ | ...                                  | 7238                                  | $1.99 \times 10^8$       |
| PKS 0925-203 | 0.348 | 16.35 | $2.25 \times 10^{45}$                          | 0.70                 | $1.87 \times 10^{26}$         | $5.61 \times 10^2$ | 2611                                 | 2217                                  | $2.90 \times 10^8$       |
| PKS 1016-311 | 0.794 | 17.58 | $4.28 \times 10^{45}$                          | 0.65                 | $1.03 \times 10^{27}$         | $1.62 \times 10^3$ | 3416                                 | ...                                   | $7.79 \times 10^8$       |
| PKS 1020-103 | 0.196 | 15.07 | $2.19 \times 10^{45}$                          | 0.49                 | $3.93 \times 10^{25}$         | $1.21 \times 10^2$ | 7920                                 | 6138                                  | $2.62 \times 10^9$       |
| PKS 1034-293 | 0.312 | 15.94 | $2.60 \times 10^{45}$                          | 1.51                 | $3.21 \times 10^{26}$         | $8.30 \times 10^2$ | 3463                                 | ...                                   | $5.65 \times 10^8$       |
| PKS 1036-154 | 0.525 | 21.8  | $3.57 \times 10^{43}$                          | 0.78                 | $5.03 \times 10^{26}$         | $9.47 \times 10^4$ | 5216                                 | 3671                                  | $6.38 \times 10^7$       |
| PKS 1101-325 | 0.355 | 16.45 | $2.14 \times 10^{45}$                          | 0.73                 | $2.04 \times 10^{26}$         | $6.42 \times 10^2$ | 3135                                 | 2949                                  | $4.04 \times 10^8$       |
| PKS 1106+023 | 0.157 | 18.01 | $9.22 \times 10^{43}$                          | 0.50                 | $2.54 \times 10^{25}$         | $1.85 \times 10^3$ | ...                                  | 2632                                  | $4.52 \times 10^7$       |
| PKS 1107-187 | 0.497 | 22.44 | $1.76 \times 10^{43}$                          | 0.50                 | $2.86 \times 10^{26}$         | $1.09 \times 10^5$ | ...                                  | 2361                                  | $1.14 \times 10^7$       |
| PKS 1128-047 | 0.266 | 21.41 | $1.21 \times 10^{43}$                          | 0.90                 | $1.37 \times 10^{26}$         | $7.63 \times 10^4$ | ...                                  | 2186                                  | $7.52 \times 10^6$       |
| PKS 1136-135 | 0.557 | 16.3  | $6.43 \times 10^{45}$                          | 2.22                 | $1.63 \times 10^{27}$         | $1.70 \times 10^3$ | 2275                                 | 2731                                  | $4.60 \times 10^8$       |
| PKS 1200-051 | 0.381 | 16.42 | $2.55 \times 10^{45}$                          | 0.46                 | $1.49 \times 10^{26}$         | $3.94 \times 10^2$ | 2361                                 | 1803                                  | $2.59 \times 10^8$       |
| PKS 1226+023 | 0.158 | 12.93 | $1.01 \times 10^{46}$                          | 40.0                 | $2.05 \times 10^{27}$         | $1.37 \times 10^3$ | 4040                                 | ...                                   | $1.98 \times 10^9$       |
| PKS 1237-101 | 0.751 | 17.46 | $4.23 \times 10^{45}$                          | 1.13                 | $1.58 \times 10^{27}$         | $2.52 \times 10^3$ | 5392                                 | ...                                   | $1.93 \times 10^9$       |
| PKS 1254-333 | 0.190 | 17.05 | $3.31 \times 10^{44}$                          | 0.54                 | $4.06 \times 10^{25}$         | $8.25 \times 10^2$ | 7800                                 | ...                                   | $6.78 \times 10^8$       |
| PKS 1302-102 | 0.286 | 15.71 | $2.68 \times 10^{45}$                          | 1.0                  | $1.77 \times 10^{26}$         | $4.45 \times 10^2$ | 3417                                 | 2439                                  | $5.61 \times 10^8$       |
| PKS 1352-104 | 0.332 | 17.6  | $6.43 \times 10^{44}$                          | 0.98                 | $2.37 \times 10^{26}$         | $2.49 \times 10^3$ | 2814                                 | ...                                   | $1.40 \times 10^8$       |
| PKS 1359-281 | 0.803 | 18.71 | $1.55 \times 10^{45}$                          | 0.67                 | $1.09 \times 10^{27}$         | $4.72 \times 10^3$ | 1889*                                | ...                                   | $1.17 \times 10^8$       |
| PKS 1450-338 | 0.368 | 22.52 | $8.61 \times 10^{42}$                          | 0.54                 | $1.63 \times 10^{26}$         | $1.27 \times 10^5$ | ...                                  | 1824                                  | $4.14 \times 10^6$       |
| PKS 1509+022 | 0.219 | 19.83 | $3.44 \times 10^{43}$                          | 0.54                 | $5.46 \times 10^{25}$         | $1.07 \times 10^4$ | 6551                                 | ...                                   | $9.80 \times 10^7$       |
| PKS 1510-089 | 0.362 | 16.21 | $2.78 \times 10^{45}$                          | 3.25                 | $9.46 \times 10^{26}$         | $2.29 \times 10^3$ | 2796                                 | ...                                   | $3.86 \times 10^8$       |
| PKS 1546+027 | 0.415 | 18.54 | $4.34 \times 10^{44}$                          | 1.42                 | $5.53 \times 10^{26}$         | $8.56 \times 10^3$ | 3893                                 | 2831                                  | $2.04 \times 10^8$       |
| PKS 1555-140 | 0.097 | 16.99 | $8.77 \times 10^{43}$                          | 0.83                 | $1.57 \times 10^{25}$         | $1.20 \times 10^3$ | ...                                  | 2001                                  | $2.53 \times 10^7$       |
| PKS 1706+006 | 0.449 | 22.8  | $1.02 \times 10^{43}$                          | 0.38                 | $1.75 \times 10^{26}$         | $1.16 \times 10^5$ | ...                                  | 2086                                  | $6.08 \times 10^6$       |
| PKS 1725+044 | 0.296 | 18.2  | $2.90 \times 10^{44}$                          | 1.21                 | $2.30 \times 10^{26}$         | $5.33 \times 10^3$ | 2638                                 | 2399                                  | $7.07 \times 10^7$       |
| PKS 1954-388 | 0.626 | 17.82 | $2.04 \times 10^{45}$                          | 2.0                  | $1.89 \times 10^{27}$         | $6.21 \times 10^3$ | 3293                                 | ...                                   | $4.32 \times 10^8$       |
| PKS 2004-447 | 0.240 | 18.09 | $2.07 \times 10^{44}$                          | 0.65                 | $7.96 \times 10^{25}$         | $2.59 \times 10^3$ | 1939                                 | 1602                                  | $3.01 \times 10^7$       |
| PKS 2059+034 | 1.012 | 17.64 | $6.90 \times 10^{45}$                          | 0.75                 | $2.02 \times 10^{27}$         | $1.97 \times 10^3$ | 3815                                 | ...                                   | $1.36 \times 10^9$       |
| PKS 2120+099 | 0.932 | 20.16 | $5.65 \times 10^{44}$                          | 0.5                  | $1.13 \times 10^{27}$         | $1.34 \times 10^4$ | 3083                                 | ...                                   | $1.54 \times 10^8$       |
| PKS 2128-123 | 0.499 | 15.97 | $6.88 \times 10^{45}$                          | 2.0                  | $1.16 \times 10^{27}$         | $1.13 \times 10^3$ | 4652                                 | 4220                                  | $2.02 \times 10^9$       |
| PKS 2143-156 | 0.698 | 17.24 | $4.41 \times 10^{45}$                          | 0.82                 | $9.80 \times 10^{26}$         | $1.49 \times 10^3$ | 836                                  | ...                                   | $4.78 \times 10^7$       |
| PKS 2329-415 | 0.671 | 18.2  | $1.67 \times 10^{45}$                          | 0.47                 | $5.15 \times 10^{26}$         | $2.07 \times 10^3$ | 4952                                 | ...                                   | $8.49 \times 10^8$       |

\*H $\gamma$  FWHM, no data for H $\alpha$  and H $\beta$  available

Table 2: Average  $H\beta$  FWHMs for flat spectrum and steep spectrum quasars from Gu, Cao, & Jiang (2001)

|                | mean (km s <sup>-1</sup> ) | median (km s <sup>-1</sup> ) |
|----------------|----------------------------|------------------------------|
| Flat Spectrum  | 3632                       | 3600                         |
| Steep Spectrum | 5240                       | 4500                         |